energies

MDPI

Article

Numerical Investigations of the Vertical Axis Wind Turbine with Guide Vane

Krzysztof Kołodziejczyk * and Radosław Ptak

Department of Power Systems and Environmental Protection Facilities, Faculty of Mechanical Engineering and Robotics, AGH University of Science and Technology, Mickiewicz Alley 30, 30-059 Krakow, Poland
* Correspondence: krzysztof.kolodziejczyk@agh.edu.pl

Abstract: More than ever, the generation of energy from renewable sources has become one of the most critical and challenging areas of human activity. This is the result of a number of factors acting simultaneously, including the highly publicized greenhouse effect, the need to reduce CO_2 emissions, the dwindling of natural resources and thus the need to protect them, including the preservation of wealth (among other natural resources) for future generations. This paper presents a numerical investigation of the operation of a vertical axis wind turbine with guide vanes. The work analyzes the obtained power on the turbine rotor for different numbers of rotor blades and different numbers of guide vanes, as well as for different proportions of the width of the rotor ring and the guide ring. The analyses carried out point to the potential feasibility of using this type of design in practice. The obtained power coefficient is higher than that of classical vertical axis wind turbines. The analyses also indicate that the proposed design solution can be optimized to increase the efficiency of wind energy extraction.

Keywords: cross-flow wind turbines; guide vanes; power coefficient; vertical axis wind turbine

check for updates

Citation: Kołodziejczyk, K.; Ptak, R. Numerical Investigations of the Vertical Axis Wind Turbine with Guide Vane. *Energies* **2022**, *15*, 8704. https://doi.org/10.3390/en15228704

Academic Editor: Ying-Yi Hong

Received: 11 October 2022
Accepted: 15 November 2022
Published: 19 November 2022

Publisher's Note: MDPI stays neutral with regard to jurisdictional claims in published maps and institutional affiliations.

Copyright: © 2022 by the authors. Licensee MDPI, Basel, Switzerland. This article is an open access article distributed under the terms and conditions of the Creative Commons Attribution (CC BY) license (https://creativecommons.org/licenses/by/4.0/).

1. Introduction

The Paris Agreement, which crowned the 21st United Nations Conference, calls for limiting greenhouse gas emissions so that the global temperature increase does not exceed 1.5 °C above pre-industrial levels, which implies a drastic reduction in the use of fossil fuels [1]. Rising raw materials prices and increasing availability problems are just some factors driving the growing interest in renewable energy sources. Dwindling natural resources, the need to reduce CO_2 emissions, and other environmental issues are driving developers worldwide to create new and more advanced renewable energy sources, the most advanced of which are photovoltaics, ocean and tidal energy, hydropower and wind power [2].

Wind and solar power are the fastest-growing renewable energy sources, growing 35% yearly [3]. The most popular wind power generators are horizontal wind turbines (HAWAT) [4]. Their main advantage is the high Cp [5] power factor of 0.4 to 0.5 [6]. In addition, HAWT designs allow for very tall structures [4] making it possible to use rotors of very large diameters. Therefore it is possible to create relatively powerful units [4]. These structures, however, are not without their drawbacks, such as landscape pollution and noise pollution [7], which have resulted in restrictions on their siting, particularly the need to keep a distance from human-inhabited spaces. The depletion of land available for new investments—wind farms—has led to the development of off-shore solutions [8] and increased interest in less human-intensive construction solutions, such as vertical axis turbines (VAWTs) [9–16]. Their low efficiency is among the biggest problems with standard vertical axis wind turbine designs. One way to increase the Cp is to introduce Omni-Directional Guide Vanes (ODGVs); such a solution increases efficiency from single-digit to high double-digit percentages [10].

It should also be mentioned here that Darrieus vertical direct-drive power plants with high capacities can be competitively priced with higher reliability than HAWTs [17]. Moreover, H-rotor power plants with the same power as HAWTs generate less overturning torque at the base. This allows a vertical-axis turbine with a power output approximately 30% higher than a HAWT to be mounted on the same platform, which generates further savings [18]. On the other hand, design solutions that are less disruptive to people and the terrestrial environment are being sought, options that could be installed closer to residential buildings [19]. One such solution is the free-running vertical axis wind turbines [20–22]. A lot of research has been done to optimize the shape of the turbine blade [23–25].

The use of guide vanes in wind turbines is not well explored, and it is an issue that is still being developed [18]. There are studies that have investigated whether the use of guide vanes would reduce the adverse effects of "negative pressure" [26]. Studies have been carried out by examining turbine performance for different configurations of guide vanes [18]. The research shows that using air deflection blades reduces the effect of the incoming wind flow on the return blades and increases the pressure on the driving blades [9,10].

Even in a classic Savonius turbine, the use of air guides has a positive effect on the operation of the power plant [10,26]. The appropriate geometry of the guide and turbine vanes allows the incoming airflow to be guided onto the turbine vanes and the braking effect of the returning blades to be neutralized [11]. There are studies in the literature where researchers have succeeded in increasing the power coefficient of VAWT with straight guide vanes by several tens to as much as 150% [27], indicating the great potential of such a solution. In addition, research has been carried out on curved guide vanes achieving efficiency gains of several tens of percent with respect to a straight vane system [28]. The research also indicates lower power output for turbine with fewer guide vanes [29]. Additionally, the investigations of cross-flow wind turbine with wind-collecting casing with two flow deflectors to increase the output power were carried out [30]. The use of deflectors in the cross-flow turbine allowed for a 60% increase in performance. The use of guide vanes to guide the flow to the Savonius turbine increased the Cp to 26% compared to the Cp that was produced without the installation of the guide vanes [31].

This paper presents a series of numerical analyses of a vertical wind turbine with air guides. Such turbines usually achieve a power coefficient less than 0.2 [18]. The use of guide vanes makes it possible to increase the power coefficient, which for the turbine under study exceeds 0.2. The power coefficient obtained is much lower than that achieved in commonly used horizontal axis turbines. It should be noted here, however, that the turbine under study with guide vanes shows a significant optimization potential. The solution analyzed is an unusual, modified proposal for a vertical axis turbine. As a result, it will have the advantages of a vertical axis turbine, i.e., relatively quiet operation, no wind guide [32], performing very well in variable winds, including variable inflow direction (in difficult wind conditions, such as on a roof) [33]. In addition, the turbine discussed in this paper has a high take-off torque and a higher power coefficient than typical vertical axis turbines. The rotating elements are shielded, which further widens its scope and makes it safer for birds, making it an interesting research object.

The numerical simulations presented in this paper extend the research conducted by analyzing the operation of a turbine with vanes for a large number of vanes and rotor blades (several dozen). An element not analyzed so far is the search for the influence of the number of guide vanes and rotor blades on the obtained power factor, including the verification of correlations in this system. The second element analyzed is the analysis of the influence on the Cp factor by the width of the rings with the guide vanes and the rotor blades.

2. Materials and Methods

The study included numerical simulations of the operation of a vertical-axis wind turbine with guide vanes, one stage of which is shown in Figure 1. The numerical studies

were aimed at analyzing the wind turbine operation in question and determining the geometric and operating parameters that would allow the maximum value of the Cp coefficient to be achieved. The geometric parameters of the turbine analyzed include modification of the ratio of rotor diameter to the diameter of the ring of vanes, with the constant outer diameter of the turbine. The second analyzed area was the various combinations of the number of blades on the vanes side and the number of blades on the rotor side. A single analysis included a numerical simulation of the airflow through the turbine with given parameters to determine the turbine shaft torque values and the turbine power.

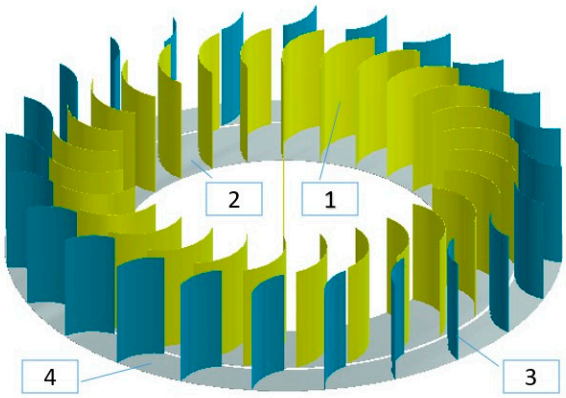

Figure 1. Construction of one turbine stage: 1. turbine blades. 2. inner ring of turbine blades. 3. guide vanes. 4. outer ring forming the blade set.

The vertical-axis wind turbine in question has been fitted with guide vanes. From a mechanical point of view, such a wind turbine is made up of two rings, one inside the other (Figure 1). The outer ring, equipped with blades guiding the air to the turbine, forms the guide vanes assembly. The inner ring of blades, connected to the generator shaft, comprises the cross-flow turbine. From above and below, the rings are connected by a lattice structure equipped with a turbine-bearing system.

Numerical simulations were carried out in the Ansys FLUENT software package. To reduce the size of the numerical model and simplify the analyses, the simulations were performed for a flat 2D system. A model representing the turbine geometry in a plane perpendicular to the axis of rotation was analyzed. This simplification, on the one hand, does not allow the influence of structural elements on the operation of the entire system to be taken into account, but on the other hand, does not introduce additional distortions. The computational domain was divided into two areas, a stationary zone comprising the guide vanes and a rotating zone. The dimensions of the computational domain are included in the diagram of Figure 2, as multiples of the turbine's outer diameter D of 2.5 m.

The resulting geometry was partitioned with a mesh consisting of hexahedral elements, compacted in the turbine zone, including the applied mesh compaction in the area of the blades and rotor blades (Figure 3).

The final model for which calculations were carried out consisted of approximately 250,000 grid elements. The computational domain was divided into five areas with different grid densities ranging from 0.3 m in the outer zone to grid densities in the blades and the turbine rings area, where the element size was no more than 0.01 m. In addition, a wall layer (inflation) consisting of 0.004 m elements was applied in the rotor blade wall zone and the blades. The final grid size was determined after conducting a sensitivity analysis of the solution to the size of the grid elements. Comparative analysis of the results obtained with the models was performed after the grid contraction of approximately 20%. The relative differences between the results obtained, before and after compaction of the grid, did not exceed a value of 2‰. Further grid compaction was therefore considered pointless, as it did not affect the result.

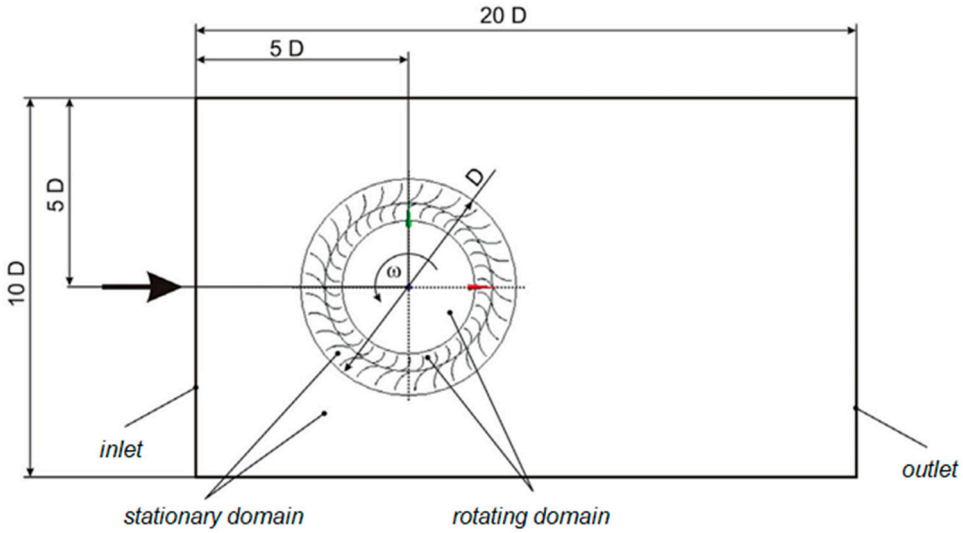

Figure 2. Computational domain scheme. This is not a scaled drawing. On the left—inlet. On the right—outlet. On the outside—stationary domain, inside—rotating domain.

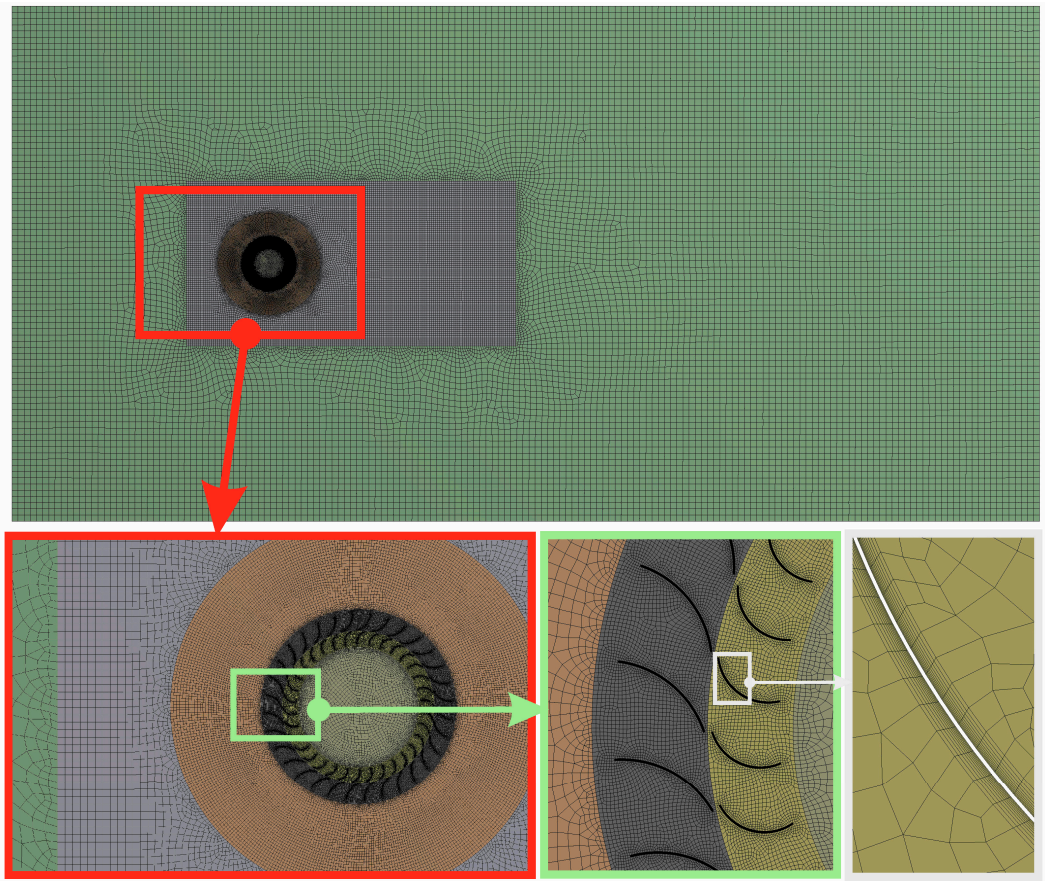

Figure 3. Computational mesh in the domains with details of refinement in the blade vicinity presented in the successive magnifications.

The medium flowing through the turbine was air at 20 °C with constant parameters, density 1.225 kg/m^3 and kinematic viscosity 1.7894 $\times$ 10^{-5} kg/(m·s). The k-omega SST turbulence model was used in the analyses carried out [34]. The k-epsilon model was also taken into account in the preliminary studies and analyses; however, due to its higher degree of accuracy, and higher stability, the k-omega SST model was finally used [20].

3. Results

3.1. Analysis of the Work of the Base Structure

The first stage of the work was to determine the turbine power characteristics as a function of the tip speed ratio for different incoming wind speeds. Simulations were carried out for incoming air velocities of 4 m/s, 8 m/s and 12 m/s defined as the boundary condition at the input to the computational domain (Figure 2). At the output, a free outflow was modeled by assigning a relative static pressure of 0 Pa, with a defined reference pressure of 1 at. A frictionless wall was defined on both sides of the computational domain by setting a wall-free sleep boundary condition. The turbine rotor was modeled by defining a rotating frame covering both the rotor blade area and the inner zone. Analyses were performed for different values of the tip speed ratio λ, resulting from rotor speed values ranging from 0 to 12 rad/s.

The analyses were carried out as steady-state simulations. The initially assumed level of convergence was the residual value of 10^{-4}. The analyses showed that such a convergence level could only be achieved for low velocity values at the inlet. In order to determine the reason why the calculations did not converge, the speed distribution was also analyzed (Figures 4 and 5). On the velocity distributions, we can observe a decrease in velocity in front of the turbine, an increase in velocity on the sides of the turbine and, most importantly, a variable velocity distribution in the area of the blades and turbine. The distributions for the lower values of the tip speed ratio (Figure 4) show a characteristic aerodynamic shadow. On the other hand, for higher values of the tip speed ratio (Figure 5), an aerodynamic shadow is also created, but with the swirls.

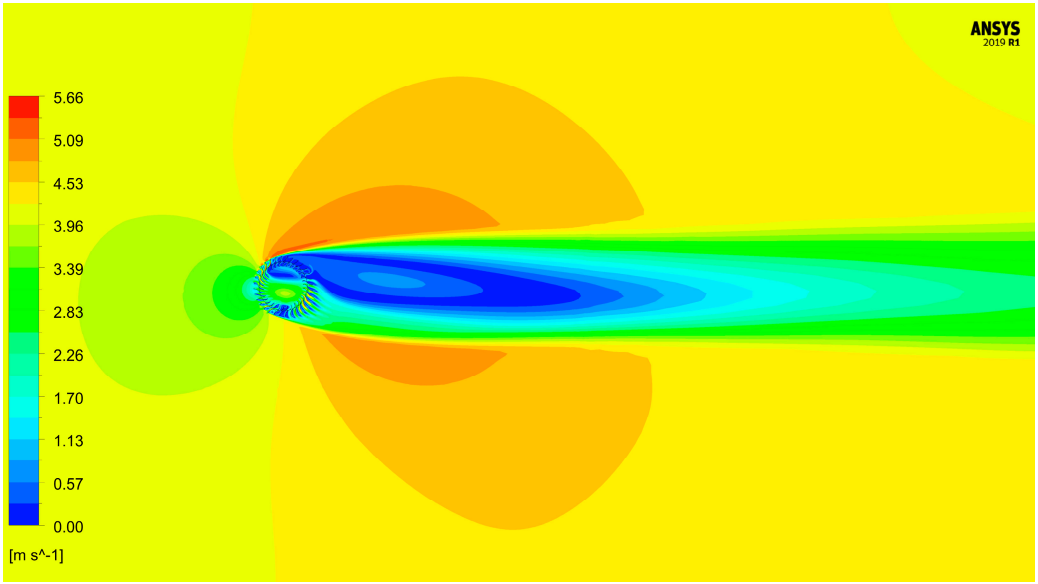

Figure 4. Distribution of velocity [m/s] for lower TSR values.

As the velocity at the inlet to the system increased, turbulence appeared behind the wind turbine, making it impossible to achieve the assumed convergence level of the calculations.

In seeking a solution to this problem, mesh compaction was introduced during the calculation, which unfortunately did not completely eliminate the problem. Finally, it was decided to introduce torque monitoring, which was chosen as the most crucial factor in determining the validity of the subject analysis. In further analyses, it was decided to introduce torque monitoring, which was chosen as the most important factor in monitoring the convergence process. Figure 6 shows the change in torque values for the following iterations.

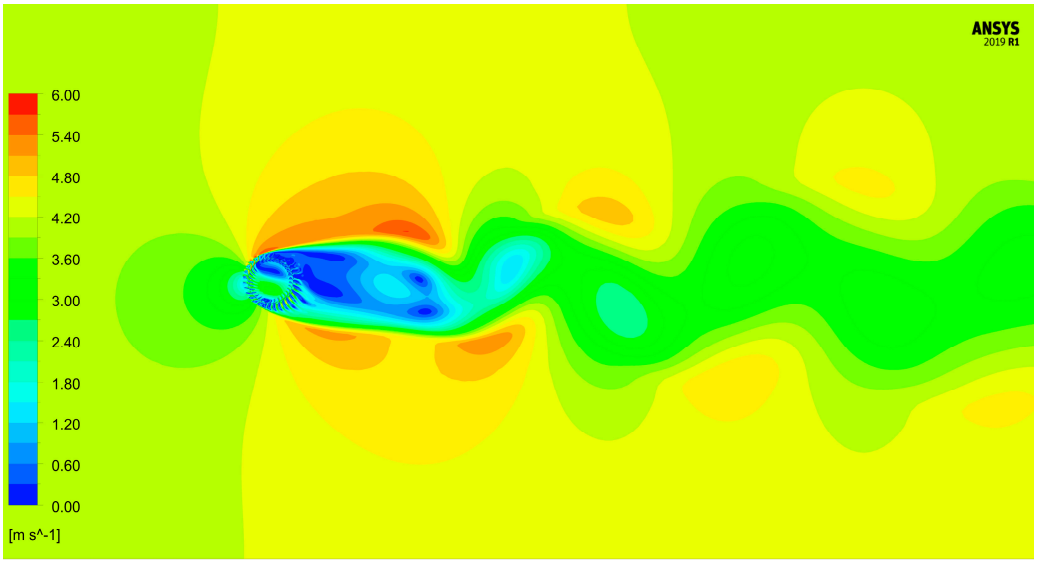

Figure 5. Distribution of velocity [m/s] for higher TSR values.

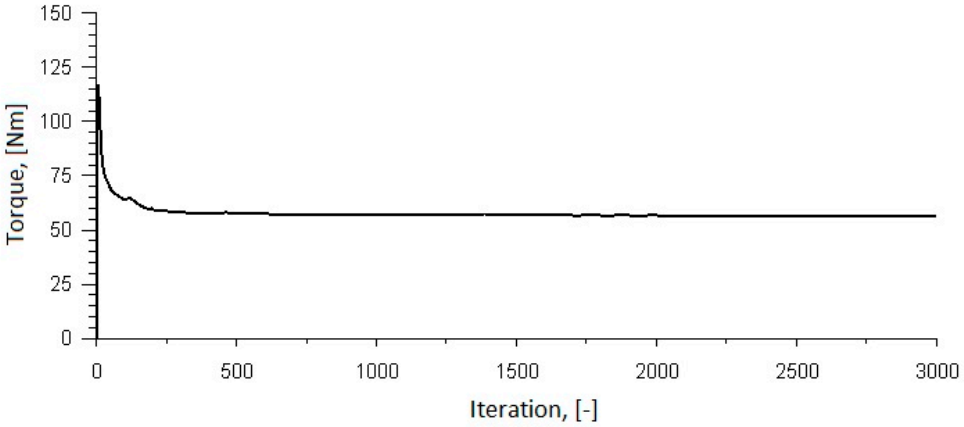

Figure 6. Change of torque values in [Nm] for the following iterations.

In addition, a calculation was carried out to check the value of the torque every 500 iterations, as shown in Table 1.

Table 1. Change in torque values for successive iterations.

Number of Iteration	1000	1500	2000	2500	3000
Torque [Nm]	57.4	57.1	57.1	56.9	56.9

After analyzing the data, as shown in Table 2, it was decided to proceed with the study despite no convergence of residuals was reached since the measurement error of the torque value does not exceed 1%.

Wind turbines, built by contractors worldwide, differ in their engineering, size, turbine speed and variation in incoming wind speed. Interchangeable sizes are used to compare turbines of different designs. The tip speed ratio (λ) is used to compare turbine speeds. This is the ratio of the blade's tip's peripheral speed to the average wind speed over the turbine. This ratio allows comparison of rotor speeds regardless of rotor diameter. In contrast, the power coefficient Cp is used to compare the power output of turbines of different sizes. This is the quotient of the power generated by the turbine to the power of the wind stream arriving at the turbine. The juxtaposition of these two quantities allows a so-called power characteristic to be created.

Table 2. Variability characteristics of the torque generated by the turbine rotor.

Minimal result	56.9
Maximal result	57.4
Range of results	0.519
Average score	57.1
Median	57.1
Standard deviation	0.207
Mean squared error	0.37%

As a result of the simulations, the dependence of the power coefficient Cp on the velocity discriminant was obtained for three values of 4, 8, 12 m/s of incoming wind speed, as shown in (Figure 7). The maximum values of the power coefficient are obtained in the range from 0.4 to 1. From the results obtained, it can be concluded that the value of the Cp coefficient is independent of the inflowing wind speed; only slight differences are obtained, a slight decrease for the lowest inflowing airspeed.

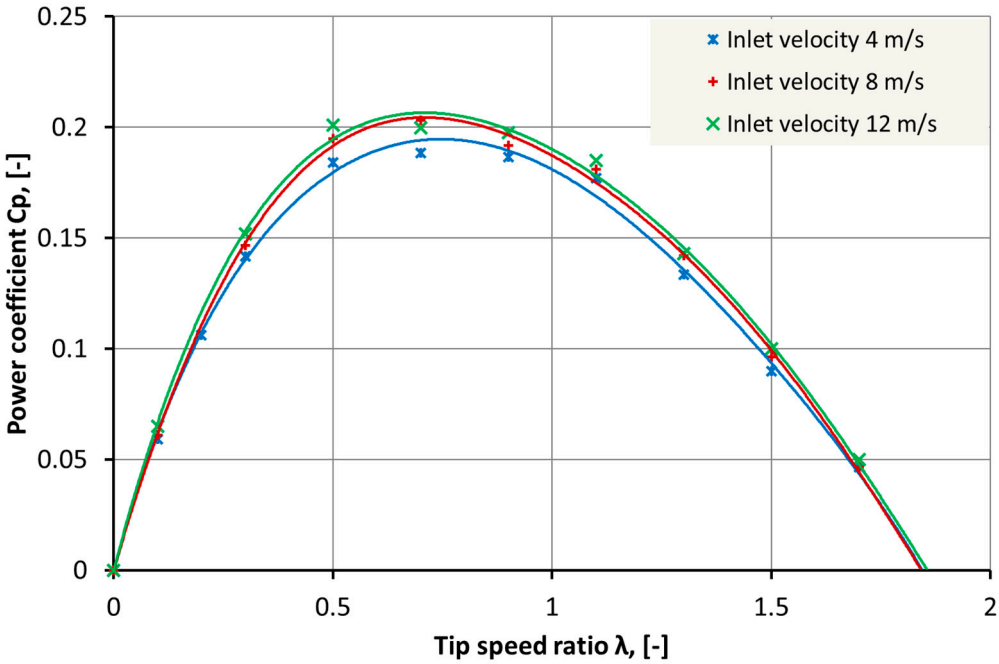

Figure 7. The change in power coefficient value depends on the TSR for different values of inflowing air velocity.

Figure 8 also shows the torque variation on rotor speed, assuming an incoming air velocity of 8 m/s. The graph clearly shows the high starting torque of the turbine. This confirms that the turbine can already be operated at very low air speeds.

When analyzing the operation of a vertical axis turbine with air blades, it is also necessary to analyze the flow of the medium through the blade system and the turbine rotor. This analysis will allow one to see how the flow through the turbine is realized and will give an overview of the turbine's operating mechanism. By analyzing the velocity distribution in the area of the air vanes and the turbine rotor (Figure 9), we can identify some areas:

- The inflow zone, where the vanes guide the flowing stream onto the turbine blades;
- The transition zone with no flow;
- The outflow zone of the stream from the rotor area;

- The blade-return zone in which the guide vanes shield the rotor blades, which are moving against the main flow. This effect reduces the negative effect of the returning rotor blades in contrast to the Savonius turbine.

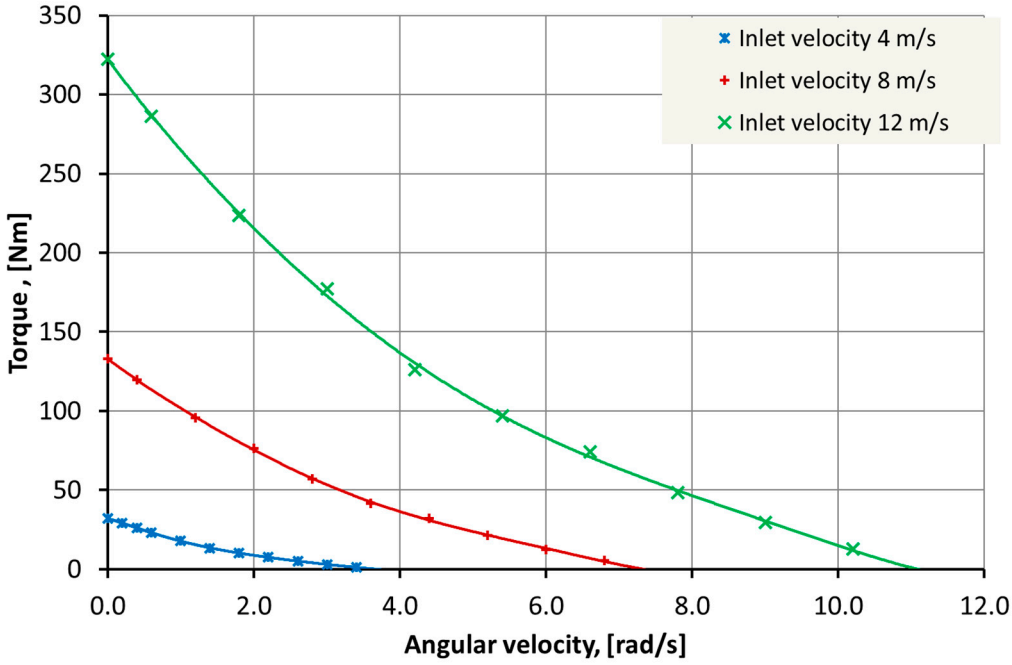

Figure 8. Dependence the torque on rotor angular velocity for an incoming air velocity: 4 m/s, 8 m/s and 12 m/s.

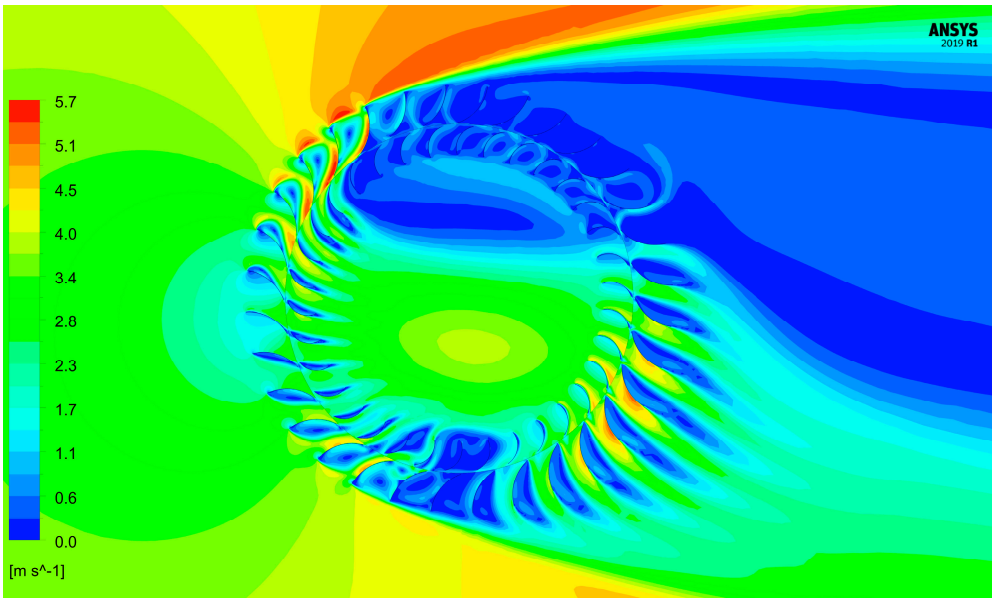

Figure 9. Distribution of velocity [m/s] in rotor zone.

In addition to the velocity distributions, pressure distributions were also obtained (Figure 10). These clearly indicate that the rotation of the turbine is caused both by the effect of the hydrodynamic force on the blade (which occurs in the inflow zone as in classical Savonius turbines) and by the pressure difference between the two sides of the turbine blade (which occurs in the outflow zone).

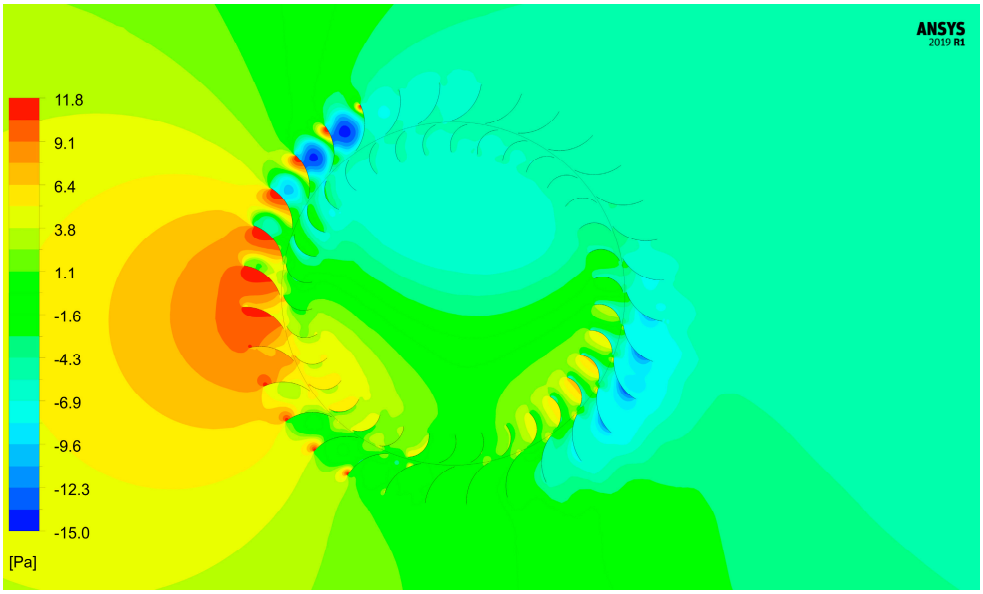

Figure 10. Distribution of relative pressure [Pa] in rotor zone.

3.2. Analysis of Turbine Operation for Different Proportions of Rotor Ring and Vanes

One of the aims of the analyses carried out was to verify how the width of the guide vanes ring and the rotor ring affect the power plant operation. An additional objective was to check the correlation for different ring width ratios. The geometrical parameter that was kept constant in all simulations was the outer diameter of the guide vanes ring (that means the outer diameter of the turbine). The geometrical parameter that was kept constant in all simulations was the outer diameter of the guide ring

This assumption allowed the obscuring field of the incoming flow to remain constant. That is, it made it possible to compare the performance of different solutions.

Flow simulations were carried out for the analysis parameters determined for the baseline solution, except that one inlet velocity value fixed at 8 m/s and one vortex zone velocity of 2.8 rad/s, corresponding to a tip speed ratio of 0.7, were used.

The air deflector consists of two rings, an outer and an inner ring, which connect the blades that guide the air to the turbine rotor. Similarly, the turbine also consists of an upper and lower ring to which the blades are attached, whose task is to convert the momentum of the airflow into turbine torque. The characteristic values of the steering wheel ring, as well as the turbine ring, are their outer and inner diameters marked from outside to inside D_{ZK}, D_{WK}, D_{ZT} and D_{WT}, respectively (Figure 11). Disregarding the small gap necessary for the correct operation of the power plant, it can be concluded that the inner diameter of the steering wheel and the outer diameter of the turbine are identical in size and are referred to hereafter as the pitch diameter D_P.

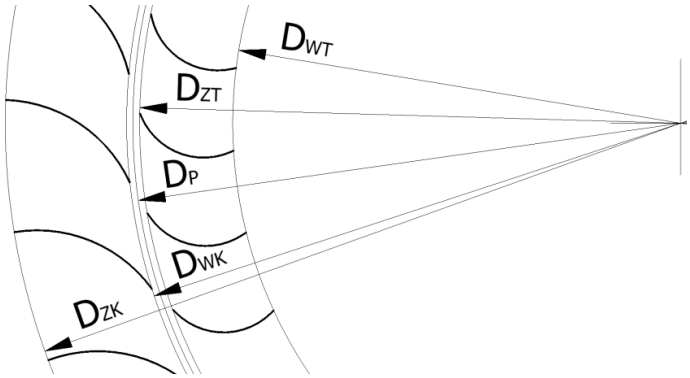

Figure 11. Arrangement of blades and turbine blades.

In this experiment, we were first interested in the relative widths of the two rings, the airfoils and the turbine, relative to their outer diameters, hereafter referred to as the α-factor (1). The second factor we were interested in was the ratio of the width of the ring of air vanes to the width of the two rings, hereafter referred to as β (2). The following formulae can express these relationships:

$$\alpha = \frac{D_{WT}}{D_{ZK}} \quad (1)$$

$$\beta = \frac{D_{ZK} - D_P}{D_{ZK} - D_{WT}} \quad (2)$$

The relative width β of the vanes' ring was tested over a range of values from 17% to 57%. Above 57%, the model did not convert properly, while values below 17% are the same as a turbine without runners, which is not the subject of this work. It should be mentioned, however, that for the same area of inflow airflow, a power plant of this design equipped with appropriate guide vanes generates a higher torque than a power plant without guides. On the other hand, the relative width α of the two rings was tested in the range of 22% to 82%. A significant drop in torque was observed below and above this range of values. The simulations were carried out according to the plan as in Table 3.

Table 3. Power coefficient Cp for different values of rotor ring widths and percentage width of guide vanes ring.

Power Coefficient Cp		**Percentage Width of Both Rings α**				
		22%	**37%**	**52%**	**67%**	**82%**
percentage guide width β	17%	0.044	0.119	0.151	0.145	0.158
	27%	0.052	0.127	0.195	0.194	0.180
	37%	0.053	0.118	0.205	0.210	0.175
	47%	0.054	0.112	0.194	0.204	0.168
	57%	0.048	0.112	0.170	0.193	0.137

In the analyzed range of variation of the width of the two rings (α) and the width of the vanes ring (β), the value of the power coefficient changes from the level of 0.044 to 0.210. As we can see, the obtained results have extremes, with a maximum value for the α factor of 67% and for the β factor of 37%.

From the graph in Figure 12, we see a greater dependence of Cp on α, where maximum values are obtained for α from 52% to 67%. At the same time, the ring widths of the guide vanes range from 37% to 47%.

3.3. Turbine Operation Analysis for Different Numbers of Rotor Blades and Vanes

The second element that was analyzed was the effect of the number of turbine blades and vanes on the wind turbine operation, including verification of their mutual correlation. Numerical simulations were carried out for initial parameters. The incoming air velocity was 8 m/s, the relative static pressure was 0 Pa at the outlet, at the sides of the full-slip wall, and the rotational domain speed was 2.8 rad/s.

The first actual working model of such a power plant was made with 34 turbine blades and 32 air guide vanes. In the conducted experiment, numerical simulations were performed for: 16, 22, 28, 34 and 40 turbine rotor blades. On the other hand, the number of guide vanes in the conducted analyses was, respectively, 8, 16, 24, 32, 40. Outside these ranges, the power coefficient decreased significantly. Obtained results of the power coefficient for different numbers of rotor blades and different numbers of guide vanes are shown in Table 4.

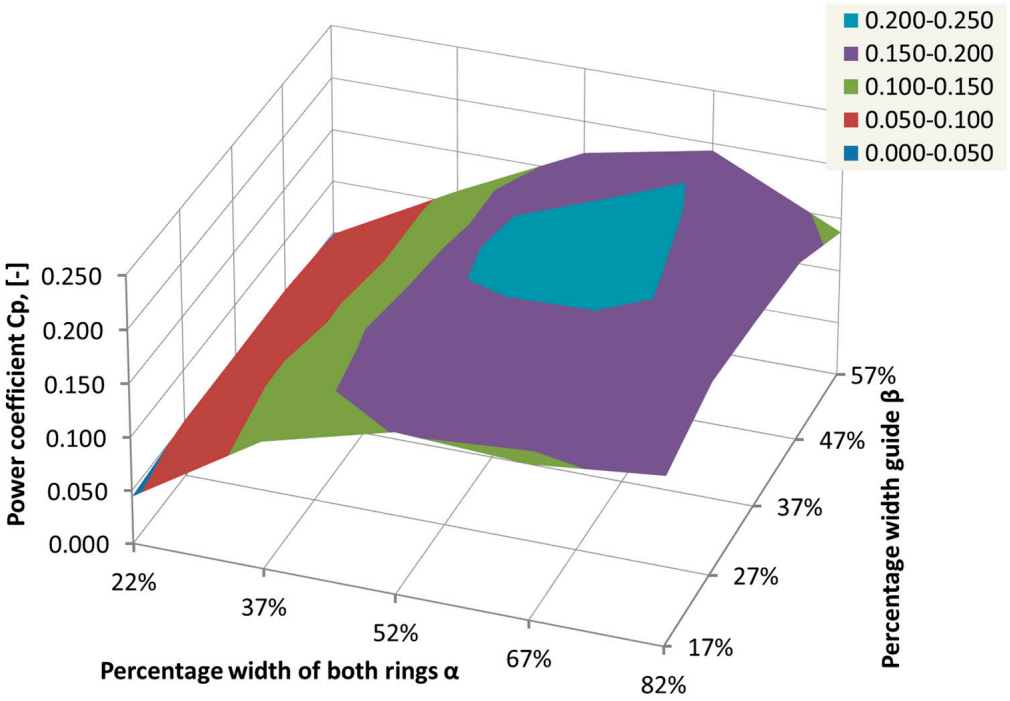

Figure 12. Dependence of the power coefficient for different proportions of the width of the guide vanes ring and the rotor ring.

Table 4. Power coefficient Cp for different numbers of rotor blades and guide vanes.

Power Coefficient Cp		Number of Turbine Blades				
		16	**22**	**28**	**34**	**40**
Number of guide vanes	8	0.140	0.181	0.163	0.145	0.165
	16	0.185	0.189	0.164	0.175	0.155
	24	0.199	0.205	0.220	0.191	0.185
	32	0.206	0.205	0.202	0.219	0.208
	40	0.185	0.197	0.192	0.197	0.208

From the results presented in Table 4, we can see that for the analyzed range of a number of blades and vanes, the value of the power coefficient varies from 0.14 to 0.22. The highest value of the power coefficient was obtained with 28 rotor blades and 24 guide vanes.

Analyzing the obtained results presented in Table 4 as well as the visualization in the form of a chart in Figure 13, we can see that we do not obtain a clear extreme for the Cp factor. At the same time, we can observe a more significant influence of the number of turbine rotor blades on the obtained Cp coefficient than the number of vanes. The highest values of Cp coefficient are obtained for the number of rotor blades from 24 to 40. Reducing the number of turbine rotor blades below 16 results in a significant reduction of the power coefficient. The effect of a reduction in Cp values is not as strongly visible when changing the number of guide vanes. This indicates that the number of guide vanes has less effect on the power achieved. From the results presented, we also see that there is no clear correlation between the number of blades on the obtained power coefficient.

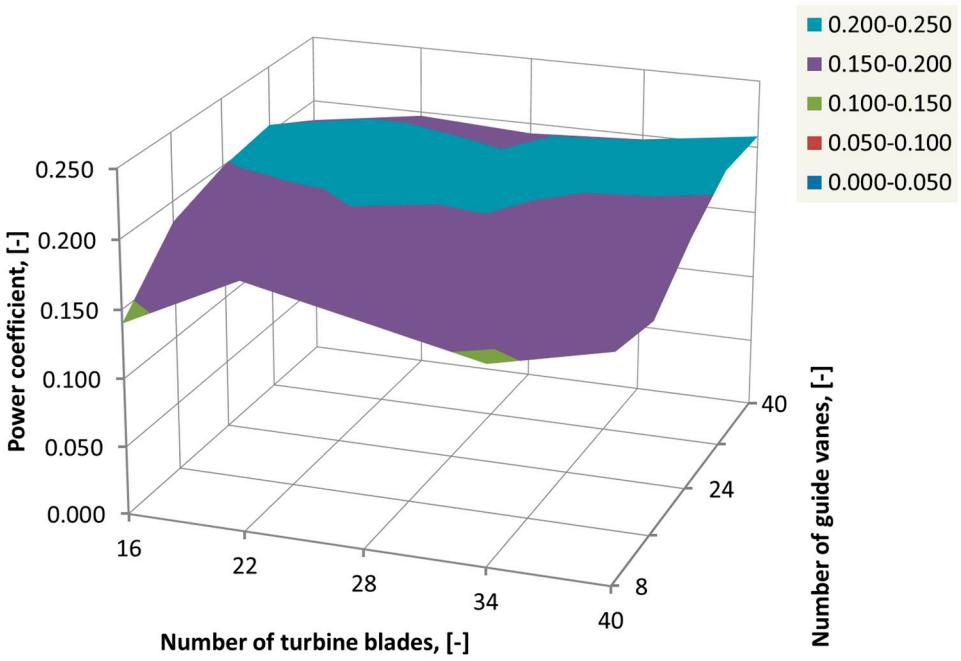

Figure 13. Dependence of the power coefficient for different proportions of the number of guide vanes and turbine blades.

4. Discussion and Conclusions

A vertical axis wind turbine equipped with guide vanes is a fascinating research object. Such a power plant has several advantages, but it also has some disadvantages. One of these features is the high starting torque shown in Figure 8, which explains why the device does not require a starter. On the other hand, the relatively low-speed range will force designers to use a multiplier, increasing the cost of such a design. However, such a turbine compensates for the low speed with relatively quiet operation. The noisy nature of high-speed horizontal axis wind turbine operation is one of the reasons for the so-called distance criterion, which significantly limits the possibility of installing wind turbines. Using guide vanes in combination with a cross-flow turbine increases the power coefficient while maintaining the same air inflow area. The guides not only direct the airflow so that it flows more efficiently over the turbine blades but also shields them from adverse effects when they move upwind. An analysis of the ratios of blade width to turbine width indicated values to generate the highest power coefficient. The maximum value of Cp was reached at 67% for the two rings' relative width s α and at 37% for the relative width of the guide β. On the other hand, the analysis of the number of guide vanes and turbine blades showed a greater variation of the power coefficient when changing the number of guide vanes than the number of turbine blades, but no less for both values took the extreme value. The power plant achieved the highest power coefficient with the number of blades of the steering ring equal to 24 and the number of blades of the turbine equal to 28.

The Cp power coefficient achieved by the turbine of 22% at the tip speed ratio of 0.7 is a good value in the group of vertical-axis wind turbines; however, horizontal-axis units achieve a power coefficient Cp above 40%, so the difference is still significant.

The turbine we are discussing still shows great optimization potential. In the near future, we will verify the geometric parameters of the guide vanes and the turbine, which will likely achieve an even higher power coefficient.

Author Contributions: Conceptualization, K.K. and R.P.; methodology, K.K.; software, K.K. and R.P.; validation, K.K.; formal analysis, R.P.; investigation, R.P.; resources, K.K. and R.P.; data curation, R.P.; writing—original draft preparation, R.P.; writing—review and editing, K.K.; visualization, R.P. and K.K.; supervision, K.K.; project administration, K.K. All authors have read and agreed to the published version of the manuscript.

Funding: AGH University of Science and Technology: IDUB No. 501.696.7997, Faculty of Mechanical Engineering and Robotics: subvention No. 16.16.130.942.

Data Availability Statement: Not applicable.

Conflicts of Interest: The authors declare no conflict of interest.

References

1. Piggot, G.; Erickson, P.; Asselt, H.; Lazarus, M. Swimming upstream: Addressing fossil fuel supply under the UNFCCC. *Clim. Policy* **2018**, *18*, 1189–1202. [CrossRef]
2. Moro, A.; Joanny, G.; Moretti, C. Emerging technologies in the renewable energy sector: A comparison of expert review with a text mining software. *Futures* **2020**, *117*, 102511. [CrossRef]
3. Yaniktepe, B.; Savrun, M.M.; Koroglu, T. Current status of wind energy and wind energy policy in Turkey. *Energy Convers. Manag.* **2013**, *72*, 103–110. [CrossRef]
4. Wiser, R.; Hand, M.; Seel, J.; Paulos, B. *Reducing Wind Energy Costs through Increased Turbine Size: Is the Sky the Limit*; Berkeley National Laboratory Electricity Markets and Policy Group, 2016; Volume 121. Available online: https://eta-publications.lbl.gov/sites/default/files/scaling_turbines.pdf (accessed on 1 November 2022).
5. Hau, E.; Renouard, H. *Wind Turbines*; Springer: Berlin/Heidelberg, Germany, 2006.
6. Khan, T.; Singh, B.; Sultan, M.T.H.; Ahmad, K.A. Performance of a HAWT Rotorwitha Modified Blade Configuration. *Pertanika J. Sci. Technol.* **2022**, *30*, 201–220. [CrossRef]
7. Filios, A.E.; Tachos, N.S.; Fragias, A.P.; Margaris, D.P. Broadband noise radiation analysis for an HAWT rotor. *Renew. Energy* **2007**, *32*, 1497–1510. [CrossRef]
8. Green, R.; Vasilakos, N. The economics of offshore wind. *Energy Policy* **2011**, *39*, 496–502. [CrossRef]
9. Wicaksono, Y.A.; Tjahjana, D.D.D.P. Computational study: The influence of omni-directional guide vane on the flow pattern characteristic around Savonius wind turbine. *AIP Conf. Proc.* **2017**, *1788*, 030016.
10. Wicaksono, Y.A.; Tjahjana, D.D.D.P.; Hadi, S. Influence of omni-directional guide vane on the performance of cross-flow rotor for urban wind energy. *AIP Conf. Proc.* **2018**, *1931*, 030040.
11. Bai, H.L.; Chan, C.M.; Zhu, X.M.; Li, K.M. A numerical study on the performance of a Savonius-type vertical-axis wind turbine in a confined long channel. *Renew. Energy* **2019**, *139*, 102–109. [CrossRef]
12. Sobczak, K.; Obidowski, D.; Reorowicz, P.; Marchewka, E. Numerical Investigations of the Savonius Turbine with Deformable-Blades. *Energies* **2020**, *13*, 3717. [CrossRef]
13. Leguizamón, S.; Avellan, F. Computational parametric analysis of the design of cross-flow turbines under constraints. *Renew. Energy* **2020**, *159*, 300–311. [CrossRef]
14. Sammartano, V.; Morreale, G.; Sinagra, M.; Collura, A.; Tucciarelli, T. Experimental Study of Cross-flow Micro-turbines for Aqueduct Energy Recovery. *Procedia Eng.* **2014**, *89*, 540–547. [CrossRef]
15. Sinagra, M.; Sammartano, V.; Aricò, C.; Collura, A.; Tucciarelli, T. Cross-flow Turbine Design for Variable Operating Conditions. *Procedia Eng.* **2014**, *70*, 1539–1548. [CrossRef]
16. Tjiu, W.; Marnotob, T.; Mata, S.; Ruslana, M.H.; Sopian, K. Darrieus vertical axis wind turbine for power generation II: Challenges in HAWT and the opportunity of multi-megawatt Darrieus VAWT development. *Renew. Energy* **2015**, *75*, 560–571. [CrossRef]
17. Matoug, C.; Augier, B.; Paillard, B.; Maurice, G.; Sicot, C.; Barre, S. An hybrid approach for the comparison of VAWT and HAWT performances for floating offshore wind turbines. *J. Phys. Conf. Ser.* **2020**, *1618*, 032026. [CrossRef]
18. Yahya, W.; Ziming, K.; Juan, W.; Al-Nehari, M.; Tengyu, L.; Qichao, R.; Alhayani, B. Study the influence of using guide vanes blades on the performance of cross-flow wind turbine. *Appl. Nanosci.* **2021**. [CrossRef]
19. Wong, K.; Chong, W.; Yap, H.; Fazlizan, A.; Omar, W.; Poh, S.; Hsiao, F. The design and flow simulation of a power-augmented shroud for urban wind turbine system. *Energy* **2014**, *61*, 1275–1278. [CrossRef]
20. Mohamed, M. Performance investigation of H-rotor Darrieus turbine with new airfoil shapes. *Energy* **2012**, *47*, 522–530. [CrossRef]
21. Sutherland, H.J.; Berg, D.E.; Ashwill, T.D. A retrospective of VAWT technology. *Sandia Natl. Lab.* **2012**, 1–64. Available online: https://www.osti.gov/servlets/purl/1035336 (accessed on 1 November 2022).
22. Castelli, M.R.; De Betta, S.; Benini, E. Effect of blade number on a straight-bladed vertical-axis Darreius wind turbine. *Int. J. Mech. Aerosp. Eng.* **2012**, *6*, 68–74.
23. Ramadan, A.; Yousef, K.; Said, M.; Mohamed, M.H. Shape optimization and experimental validation of a drag vertical axis wind turbine. *Energy* **2018**, *151*, 839–853. [CrossRef]
24. Tian, W.; Mao, Z.; Zhang, B.; Li, Y. Shape optimization of a Savonius wind rotor with different convex and concave sides. *Renew Energy* **2018**, *117*, 287–299. [CrossRef]
25. Kumar, A.; Saini, R.P. Performance analysis of a single stage modified Savonius hydro kinetic turbine having twisted blades. *Renew. Energy* **2017**, *113*, 461–478. [CrossRef]
26. Gronman, A.; Backman, J.; Hansen-Haug, M.; Laaksonen, M.; Alkki, M.; Aura, P. Experimental and numerical analysis of vaned wind turbine performance and flow phenomena. *Energy* **2018**, *159*, 827–841. [CrossRef]

27. Morshed, K.N. Experimental and Numerical Investigations o Aerodynamic Characteristics of Savonius Wind Turbine with Various Overlap Ratios. Electronic Theses and Dissertations. Master's Thesis, Graduate Faculty of Georgia Southern University, Statesboro, GA, USA, 2010; Volume 773. pp. 1–71.
28. Wong, K.H.; Chong, W.T.; Poh, S.C.; Shiah, Y.-C.; Sukiman, N.L.; Wang, C.T. 3D CFD simulation and parametric study of a flat plate deflector for vertical axis wind turbine. *Renew. Energy* **2018**, *129*, 32–55. [CrossRef]
29. Dragomirescu, A. Performance assessment of a small wind turbine with cross-flow runner by numerical simulations. *Renew. Energy* **2011**, *36*, 957–965. [CrossRef]
30. Tanino, T.; Yoshihara, R.; Miyaguni, T. A Study on a Casing Consisting of Three Flow Deflectors for Performance Improvement of Cross-Flow Wind Turbine. *Energies* **2022**, *15*, 6093. [CrossRef]
31. Mazlan, M.Z.; Mohd Zawawi, F.; Tahzib, T.; Ismail, K.; Samion, S. Performance Analysis of Highway Wind Turbine Enhanced with Wind Guide Vanes Using the Taguchi Method. *CFD Lett.* **2021**, *13*, 25–42. [CrossRef]
32. Shyu, L.S.; Lee, C.H.; Hsiao, Y.C.; Shih, T.M.; Chang, C.C.; Wang, D.Y. High-efficiency 4kW VAWT design and development. *Adv. Mater. Res.* **2012**, *512–515*, 617–622. [CrossRef]
33. Eriksson, S.; Bernhoff, H.; Leijon, M. Evaluation of different turbine concepts for wind power. *Renew. Sustain. Energy Rev.* **2008**, *12*, 1419–1434. [CrossRef]
34. Alom, N.; Borah, B.; Saha, U.K. An insight into the drag and lift characteristics of modified Bach and Benesh profiles of Savonius rotor. *Energy Procedia* **2018**, *144*, 50–56. [CrossRef]